Three-Dimensional Linear Stability Approach to Transition on Wings and Bodies of Revolution at Incidence

Tuncer Cebeci,* H. H. Chen,† D. Arnal,‡ and T. T. Huang§
California State University at Long Beach, Long Beach, California 90840

The calculation of transition on an infinite swept wing at several angles of incidence for several sweep angles and on a body of revolution at one incidence is investigated with the e^n method based on the eigenvalue formulation of Cebeci and Stewartson in which the relationship between the two wave numbers α and β are determined by making use of the saddle-point method. The method, which is based on the solution of the boundary-layer and Orr-Sommerfeld equations by a finite difference procedure, is evaluated in terms of measurements reported for the flow around a swept wing equipped with a cambered leading edge and attached to a half fuselage and for the flow around a prolate spheroid at 10-deg incidence. It is shown to be convenient to use, particularly because the neutral stability curves (zarfs) facilitate the calculation and avoid uncertainties associated with the choice of magnitude and location of the critical frequencies. In general, the calculated values of the onset of transition are in good agreement with measured values.

Introduction

A NUMBER of correlation formulas have been developed to calculate the onset of transition and have proved very useful, although it is recognized that they lack generality and can be used outside the range of flows upon which they are based only with great care. Linear stability theory and its implementation through the e^n method, as proposed by Smith and Gamberoni[1] and van Ingen,[2] and recently reviewed by Bushnell et al.,[3] offers the possibility of being able to represent the onset of transition in a wide range of flow configurations. The accuracy of the approach for incompressible flows can be assessed in terms of two-dimensional boundary layers with and without heat transfer,[4] separation bubbles,[5,6] rotating disks,[7] and yawed cylinders.[8] This paper is concerned with its application to swept wings and bodies of revolution at incidence.

The calculation method is based on the solution of the three-dimensional laminar boundary layer and linear stability equations and is described in Sec. II for an infinite swept wing and in Sec. III for a body of revolution. In the former case, the boundary-layer calculations for an infinite swept wing are solved in an inverse mode with the relationship between the inviscid and viscous flows expressed through the Hilbert integral. The resulting velocity profiles are used in the solution of the stability equation and, thereby, in the determination of the amplification rates in the e^n method to provide the location of the onset of transition. The disturbance frequency needed in the e^n method and the manner in which it is obtained and used are also considered in this section. Section III describes the procedure for a body of revolution where the boundary-layer equations are solved with a combination of standard and characteristic box methods for a prescribed inviscid pressure distribution and with a stability criterion to ensure numerical accuracy, as previously used by Cebeci and Su.[9] The resulting profiles are then used in the solution of the stability equation described in the previous section. In Sec. IV, the method is evaluated in relation to the experiments of Arnal and Juillian,[10] who reported measurements of the flow around a symmetric ONERA-D wing equipped with a cambered leading edge and attached to a half-fuselage. Results are presented for a range of sweep angles, Reynolds numbers, and angles of attack. In Sec. V, the method is evaluated in relation to the experimental data of Meier and Kreplin,[11] who measured the location of the onset of transition as well as the separation patterns on a prolate spheroid of fineness ratio of six over a range of angles of attack. The present study deals with those obtained at $\alpha = 10$ deg for a Reynolds number of 6.6×10^6. The final section of the paper provides a summary of the more important conclusions.

Received June 11, 1990; revision received Nov. 7, 1990; accepted for publication Nov. 16, 1990.

*Professor and Chairman, Aerospace Engineering Department. AIAA Fellow.

†Associate Professor, Aerospace Engineering Department. Member AIAA.

‡ONERA-CERT-DERAT, Toulouse Cedex, France.

§David Taylor Research Center, Bethesda, MD 20084.

II. Description of the Method for an Infinite Swept Wing

A. Interactive Boundary-Layer Procedure

For a laminar incompressible flow over an infinite swept wing, the boundary-layer equations are well known and can be written as

$$\frac{\partial u}{\partial x} + \frac{\partial v}{\partial y} = 0 \tag{1}$$

$$u\frac{\partial u}{\partial x} + v\frac{\partial u}{\partial y} = u_e\frac{du_e}{dx} + \nu\frac{\partial^2 u}{\partial y^2} \tag{2}$$

$$u\frac{\partial w}{\partial x} + v\frac{\partial w}{\partial y} = \nu\frac{\partial^2 w}{\partial y^2} \tag{3}$$

Usually these equations are solved subject to the boundary conditions

$$y = 0, \qquad u = v = w = 0 \tag{4a}$$

$$y = \delta, \qquad u = u_e, \qquad w = w_e \tag{4b}$$

in which $u_e(x)$ is specified in the chordwise direction of the wing. The spanwise velocity w_e is constant and obtained from the freestream velocity U_∞ and the sweep angle. The solution procedure is straightforward since the spanwise momentum equation is decoupled from the streamwise momentum equation. The solution of Eqs. (1) and (2) is essentially that of a two-dimensional flow problem and, once obtained, the second-order spanwise momentum equation (3) can be solved easily.

This procedure assumes that there is no flow separation since the solutions of the boundary-layer equations are singular at separation when they are attempted for a prescribed velocity distribution. To obtain the results of Sec. IV, we used the measured velocity distributions on the infinite swept wing of Arnal and Juillian[10] as the external boundary condition and found that the solutions of the boundary-layer equations broke down near the pressure peak due to flow separation; therefore, it was not possible to continue beyond the pressure peak. To circumvent this difficulty, it was necessary to make use of a form of the interactive boundary-layer procedure developed initially for two-dimensional flows by Cebeci et al.[12] and subsequently for quasi-three-dimensional flows by Cebeci et al.[13] In this modified procedure, the boundary-layer equations were solved in an inverse mode with successive sweeps over the wing surface. For each sweep, the external velocity w_e was assumed to be constant and equal to its inviscid velocity w_e^o, and u_e was written as the sum of the inviscid velocity $u_e^o(x)$ over the wing and a perturbation velocity $\delta u_e(x)$ given by the Hilbert integral, as described in Ref. 13. The inviscid velocity components were assumed to correspond to the experimental values. The validity of this assumption was investigated by comparing the solutions obtained with the standard method prior to breakdown and those with the inverse method. The comparison showed differences only in the third decimal place. Even though the standard method had indicated separation, those with the inverse method did not after two sweeps. This allowed us to conclude that the separation predicted by the standard method must be marginal and that the predictions of the inverse method can be regarded as equivalent to the real flow.

B. Linear Stability and the e^n Method

For two- and three-dimensional incompressible flows, the calculation on the onset of transition with the e^n method makes use of the solutions of the Orr-Sommerfeld equation

$$\phi^{iv} - 2(\alpha^2+\beta^2)\phi'' + (\alpha^2+\beta^2)^2\phi - iR(\alpha\bar{u}+\beta\bar{w}-\omega) \times [\phi'' - (\alpha^2+\beta^2)\phi] + iR(\alpha\bar{u}'' + \beta\bar{w}'')\phi = 0 \tag{5}$$

which is usually written in dimensionless form so that all velocities and lengths are normalized by a reference velocity u_o and length ℓ, with the Reynolds number R defined by $R \equiv u_o\ell/\nu$. The parameters α and β denote the wave numbers in the x and z directions, respectively, and are made dimensionless by dividing the dimensional quantities by $1/\ell$. The parameter ω represents the radian frequency and is made dimensionless by dividing by u_o/ℓ. Primes in Eq. (5) denote differentiation with respect to a dimensionless distance $\bar{y}(\equiv y/\ell)$.

For two-dimensional flows, it is common to assume that the disturbances are also two dimensional as the mean flow so that $\beta = 0$ as are the two quantities $\bar{w}$ and $\bar{w}''$. In this case, the onset of transition requires the evaluation of the integral

$$n = \int_{x_o}^{x} -\alpha_i dx \tag{6}$$

for a set of specified dimensional frequencies $\omega^*/2\pi$. With the velocity profiles $\bar{u}$ and their second derivatives $\bar{u}''$ obtained from the solution of the boundary-layer equations, the solution of Eq. (5) reduces to an eigenvalue problem involving four scalar quantities α_r, α_i, R, and ω. The numerical procedure to solve this eigenvalue problem is described in Ref. 14. It is clear that the value of R is known at any streamwise station and that the real and imaginary parts of wave number α provide two equations. Thus, solutions can be obtained provided ω is known.

With the velocity profiles known from the boundary-layer equations, the solution of Eq. (5) begins at a Reynolds number R greater than its critical value R_{cr} on the lower branch of the neutral stability curve. This provides the desired frequency that allows the solution of the eigenvalue problem in which α is computed at the subsequent Reynolds numbers and leads to one amplification curve. The process is repeated to obtain amplification curves for different values of dimensional frequency $\omega^*/2\pi$. The envelope of the resulting curves corresponds to the maximum amplification factors from which transition is obtained by assuming a value of n, commonly taken to be between 8 and 9.

This envelope procedure is useful and convenient for two-dimensional attached flows, but has limitations for more complicated flows such as those with separation (e.g., see Ref. 5) and for the three-dimensional flows of this paper. A more general method would require the determination of the first-dimensional frequency, referred to as the critical frequency, which achieves the predetermined amplification factor corresponding to transition.

For three-dimensional incompressible flows, the solution of Eq. (5), which involves five scalars α, β, ω_r, ω_i, and R in the temporal amplification theory and six scalars α_r, α_i, β_r, β_i, ω, and R in the spatial amplification theory, is considerably more difficult than its counterpart in two-dimensional flows. As in two-dimensional flows, both temporal and spatial amplification theories are used to compute transition with the e^n method. In the temporal amplification approach used by Malik,[15] the wave numbers α and β are related by the disturbance angle γ through

$$\gamma = \tan^{-1}(\beta/\alpha) \tag{7}$$

with γ assumed and the dimensional frequency $\omega_r^*/2\pi$ specified, α and β represent one unknown from Eq. (7); with R known, the second unknown is the growth rate of the disturbance ω_i. Once a solution for an assumed value of γ is obtained, additional calculations for different values of γ are made to maximize the temporal amplification rate ω_i. Mack[16] uses a spatial amplification theory and a different eigenvalue procedure in which he assumes the spanwise wave number β is real, thus allowing the wave to grow only in the chordwise direction. The value of β is obtained from the irrotationality condition applied to the complex wave number vector which, for an infinite span wing, requires that the dimensional spanwise wave number β remains constant as the wave moves downstream. With these assumptions, the problem reduces to the calculation of the complex chordwise wave number α at each chordwise position for the specified dimensional values of β and ω.

The eigenvalue procedure used here is also based on the spatial amplification theory but differs from that of Mack[16] in that the relationship between the two wave numbers α and β is not assumed but is computed by making use of concepts based on group velocity using the saddle-point method discussed by Cebeci and Stewartson[17] and Nayfeh.[18] According to this method, let us consider an oscillatory disturbance with period $2\pi/\omega^*$ generated at the origin so that the disturbance at large finite values of x,z may be assumed to be of the form

$$\tilde{Q}(x,z,y;\,t) = e^{-i\omega t}\int_C Q(\beta;\,\omega,y)e^{i(\alpha x+\beta z)}d\beta \tag{8}$$

where C is a contour in the complex plane of β, extending to ∞ in either direction, Q is a determinate function of $(\beta;\,\omega,z)$ whose properties are such that the integral converges, and α is a function of β,ω found from the solution of Eq. (5). Now for any ray in the (x,z) plane and passing through the origin, we can write

$$z = x\tan\gamma, \qquad |\gamma| \le \pi/2 \tag{9}$$

with γ denoting a constant and look for the dominant contribution to $\tilde{Q}$ along this ray as $x\to\infty$. This comes from the saddle point of $\alpha x + \beta z$, regarded as a function of β, which occurs when

$$\left(\frac{\partial\alpha}{\partial\beta}\right)_{\omega,R} + \tan\gamma = 0 \tag{10}$$

with ω,R being held constant during the differentiation. We note that, since x and z are real, the imaginary part of $\partial\alpha/\partial\beta$ must be zero to satisfy Eq. (10). Combining Eqs. (9) and (10) we can write the relation

$$\frac{\partial\alpha}{\partial\beta} = -\frac{z}{x} = -\tan\gamma \tag{11}$$

which provides the wave orientation and growth direction of the disturbance and can be used to relate the two wave numbers α and β to each other as needed in the eigenvalue problem.

We observe that with α, β defined by Eq. (11), the growth of the disturbance at (x,z) over its value at the origin is dominated by the exponential factor

$$\exp\left[-(\alpha_i x + \beta_i z)\right]$$

and, along the ray given by Eq. (11), the disturbances are damped with increasing x if the amplification rate Γ defined by

$$\Gamma \equiv \alpha_i - \beta_i \left(\frac{\partial\alpha}{\partial\beta}\right)_{\omega,R} \tag{12}$$

is >0, neutral if $\Gamma = 0$, and amplified when $\Gamma<0$. In the eigenvalue procedure used here, once α and β are computed subject to the requirements of Eq. (11), additional calculations are then made for different values of $\partial\alpha/\partial\beta$ in order to determine the maximum amplification rate Γ. In the spirit of the e^n method, the values of $\Gamma(x)$ are then integrated to find the value of n for the specified frequency. As in two-dimensional flows, this process is repeated for different dimensional frequencies to find the critical frequency that leads to the most integrated amplified amplification rate. In their use of this eigenvalue procedure for a rotating disk, Cebeci and Stewartson[19] fixed the direction of the disturbance angle γ as computed on the three-dimensional neutral stability curve and did not maximize it during the calculations but, as we shall discuss later in this paper, Γ can vary considerably with γ and must be maximized.

It is plausible to assume that, in three-dimensional flows, the e^n method calculations should begin on a neutral curve and be used to compute the dimensional frequency needed in the calculation of amplification rates, as in two-dimensional flows. The precise definition or extension of a neutral stability curve for three-dimensional flows has not, however, been formally discussed and used in the literature except in the work of Cebeci and Stewartson[17,19] who used spatial amplification theory to define this curve, which they referred to as a zarf (literally "envelope" in Turkish), as that on which disturbances neither grow nor decay at large distances from the origin of the flow in any direction. They showed that α and β have the properties

$$\alpha_i = \beta_i = 0, \qquad \frac{\partial\alpha}{\partial\beta} = \text{real} \tag{13}$$

on the zarf that, locally at least, coincides with that for temporal disturbances defined by the requirement $\omega_i = 0$ and such that over one side of its projection with the ω_r plane, $\omega_i<0$ for all α, β, whereas on the other side, $\omega_i>0$ for at least one pair of values of α, β. They recommend the use of the zarf for each ω as the origin of transition calculations in three-dimensional flows and presented zarfs for a rotating disk and for Blasius flow.[19]

As we show later in the paper, the use of zarf not only provides the frequency needed in the transition calculations but it can substantially reduce the effort required to determine the critical frequency that leads to the most amplified amplification rates. In addition, it can be used to estimate eigenvalues that are otherwise difficult to obtain.

III. Description of the Method for a Body of Revolution

The method used to solve the stability equation for a body revolution at incidence is essentially the same as that used for an infinite swept wing discussed in the previous section. The main difference is due to the calculation of boundary layers since the flow in this case is fully three-dimensional and spanwise similarity assumption used for an infinite swept wing does not apply. Also in the region where the calculations are made to determine the location of the onset of transition, there is no flow separation. As a result, it is sufficient to use a direct method. The boundary-layer method used here is the same one used by Cebeci and Su[9]; it considers the boundary-layer equations in curvilinear orthogonal coordinate system and obtains their solution with a finite difference method based on Keller's box scheme for a prolate spheroid defined by

$$\left(\frac{x}{a}\right)^2 + \left(\frac{r_o}{b}\right)^2 = 1 \tag{14}$$

subject to an external velocity distribution given by the inviscid flow theory. To avoid the singularity at the nose, ξ ($\equiv x/a$) $= -1$, in a region of $-1 \le \xi \le \xi_o$, the calculation method used the procedure of Ref. 20 which employed transformations that allow the boundary-layer equations to be solved without numerical difficulties. For $\xi > \xi_o$, the solutions of the equations were obtained by two different versions of the Keller box scheme depending on the complexity of the flow-field. In regions of the positive crossflow velocity, region A, the standard box scheme is used and the characteristic box scheme in regions of negative crossflow velocity, region B. In both cases, the calculations were started on the line of symmetry of a specified ξ location and continued toward the leeward line of symmetry with the standard box scheme in region A and the characteristic box scheme in region B, which, according to our calculations, starts at $\xi = -0.70$ on the leeward line of symmetry. In common with the results of Cebeci and Su[9] for $\alpha = 6$ deg, region B was followed by a region in which flow separation occurred. The data of Meier and Kreplin[11] showed that transition occurred before the line of separation, and it was, therefore, necessary to perform the boundary-layer calculations only within the region of attached flow.

As described in Ref. 21, the calculations made use of the procedure of Ref. 9 with two grids, grid I and II. The former corresponded to uniform step lengths in the circumferential θ and streamwise ξ directions with $\Delta\theta = 2.5$ deg and $\Delta\xi = 0.001$. The latter comprised nonuniform step lengths in both directions, as described in Ref. 21. The calculations performed with both grids showed that the solutions with grid II chosen in accordance with the stability parameter β, as discussed by Cebeci and Su[9] were accurate and free from any oscillations in wall shear parameter and were used in the stability calculations discussed in Sec. V.

IV. Results and Discussion for the Infinite Swept Wing

Before we present the results for the modified ONERA-D wing, it is useful to point out that most computational and experimental work on wings has concentrated on its attachment line. It is known, largely through experiments such as those of Pfenninger,[22] Gaster,[23] and Poll,[24] that the location of the onset of transition on the attachment line of swept wings depends on the Reynolds number based on the momentum thickness of the spanwise velocity profile. For values of this Reynolds number <240, the smallest of disturbances will ensure turbulent flow on the attachment line. For lower values, transition either occurs along the attachment line or takes place downstream of it, possibly in the region of favorable pressure gradient as a consequence of inflectional instabilities in the cross-stream velocity profiles. The sweep angle, nature of the upstream boundary layer, and flow convergence deter-

mine the local momentum thickness along the leading edge. Divergence is related to the radius of the curvature of the leading edge so that a small radius will lead to stronger divergence with consequent reduction in the momentum thickness and Reynolds number. Thus, for example, a tapered leading edge can lead to a decreasing Reynolds number and to relaminarization along the length of the attachment line.

Solution of the two-dimensional Orr-Sommerfeld equation, with the velocity profile determined from the boundary-layer equations for the attachment line, leads to a critical transition Reynolds number of 268 and, as shown in Ref. 25, inclusion of nonparallel effects lowers this value to 236, which is in agreement with experiment. The problem of performing calculations away from the attachment line involves the solution of the equations described in Sec. II to determine the location of the onset of transition on the infinite swept wing configuration investigated in the F2 wind tunnel at Le Fauga-Mauzac Center by Arnal and Juillian.[10] The numerical method used to solve the eigenvalue problem associated with Eq. (5) is similar to that described by Cebeci and Chen.[26] The model was an ONERA-D airfoil, symmetric between $x/c = 0.20$ and 1 and equipped with a cambered leading edge, so that the pressure distributions differed from those observed on the classical ONERA-D profile. The chord normal to the leading edge was 300 mm and the span was 900 mm with zero angle of sweep. The wing and the half-fuselage were mounted on a turntable. Three kinds of experiments were performed so that the pressure distribution measurements, wall visualizations by sublimation techniques, and hot-film measurements were obtained. Ten hot films were glued on the model, from 2.5 to 8.6% of chord, and recorded simultaneously for more than 100 combinations of the wind-tunnel speed, angle of sweep, and angle of attack. The positions of the hot films were chosen to avoid interactions between probes. This was verified by comparing the transition positions obtained by the hot-films records and by the wall visualization (in the absence of hot films): the results were similar. Three angles of sweep ($\lambda = 49$, 55, and 61 deg) and four angles of attack ($\alpha = 0, -2, -4$, and -8 deg) were studied.

Before we report and examine the calculated and experimental results, it is useful to discuss the procedure used to obtain the eigenvalues and to compute the dimensional frequencies needed in the e^n method. For given velocity profiles, the stability calculations begin on the zarf where, with R known and α_i, β_i zero, the eigenvalue problem consists of calculating α_r, β_r, and ω and is solved subject to the requirement that $\partial\alpha/\partial\beta$ is real. Several calculations showed that it was very important that the location where the zarf calculations were initiated was near the leading edge of the wing, where the lower branch solutions of the zarf change from positive to negative. Figure 1a shows the variation of zarf ω along the leading edge of the wing for $\lambda = 49$ deg, $V_\infty = 60$ and 85 ms^{-1} at $\alpha = 0$ deg. As can be seen, the lower branch of the ω zarf is negative with relatively flat values of ω away from the leading edge, whereas ω undergoes a very rapid variation near $x/c = 0.04$ and 0.05. Figure 1b shows that ω becomes positive and increases rapidly around $x/c = 0.04$ for $\alpha = 0$ deg, $V_\infty = 60$ ms^{-1} (Ref. 21). This behavior of ω near the leading edge is very important since the e^n method requires the calculation of the frequency, which leads to the most amplified amplification rate Γ. An accurate calculation of this frequency and its location is crucial to the accuracy of the transition location.

Upon the calculation of the eigenvalues of the zarf at a specified x/c location, the calculations proceed to the next x/c station in order to solve the eigenvalue problem for α and β for specified dimensional $\omega^*/2\pi$ frequencies determined on the zarf with the requirement that $\partial\alpha/\partial\beta$ is real and is given by its value at the previous x/c location, which amounts to specifying the disturbance angle γ. The computed values of α and β are used to calculate the amplification rate Γ according to Eq. (12), and the eigenvalue procedure was repeated for specified values of γ in order to determine the value of γ for which Γ is minimum. Once it has been determined, the calculations proceed to the next x/c station in order to compute new values of α, β so that the minimum value of Γ can be determined. The calculations for the experimental arrangement of Ref. 10 indicated that it was important to vary γ in order to minimize the amplification rate Γ and that failure to specify the direction of the disturbance computed at the zarf produced unacceptable results.

This procedure is for one value of frequency $\omega^*/2\pi$ chosen at a certain x/c location. As in two-dimensional flows, it is repeated for different values of ω computed for a zarf at different x/c locations. Since the frequency near the leading edge of the wing varies drastically, it is important to choose these x/c locations carefully. Figure 2 shows the computed frequencies and the resulting amplification factors n for four different frequencies for $\lambda = 49$ deg, $\alpha = 0$ deg, $V_\infty = 60$ ms^{-1}.

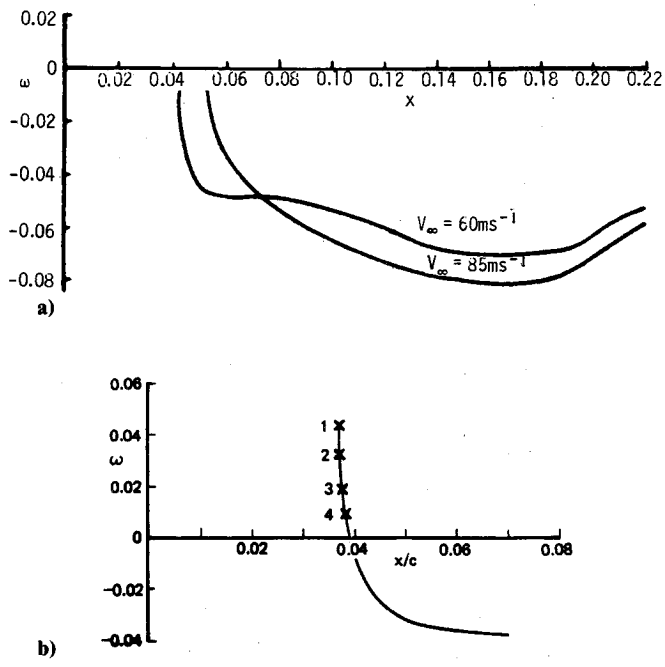

Fig. 1 Variation of ω on zarf: a) near the leading edge for $\lambda = 49$ deg, $V_\infty = 60$ and 85 ms^{-1}, $\alpha = 0$ deg; b) very close to the leading edge for $\lambda = 49$ deg, $\alpha = 0$ deg, $V_\infty = 60$ ms^{-1}.

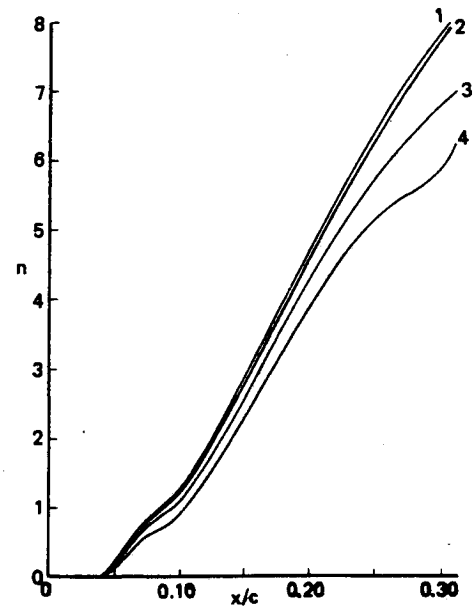

Fig. 2 Variation of the amplification factors for $\lambda = 49$ deg, $\alpha = 0$ deg, $V_\infty = 60$ ms^{-1}.

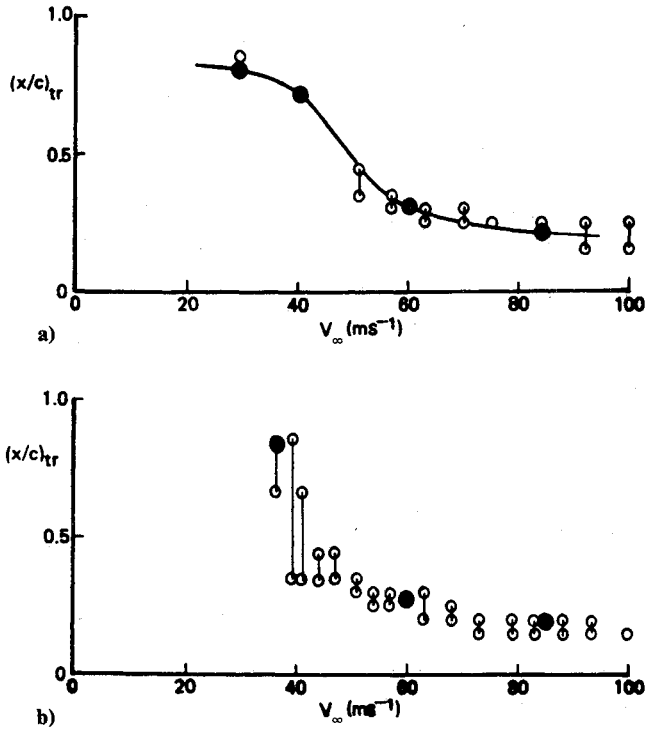

Fig. 3 Experimental (open symbols) and calculated (closed symbols) transition locations: a) $\lambda = 49$ deg, $\alpha = -2$ deg; b) $\lambda = 55$ deg, $\alpha = -2$ deg.

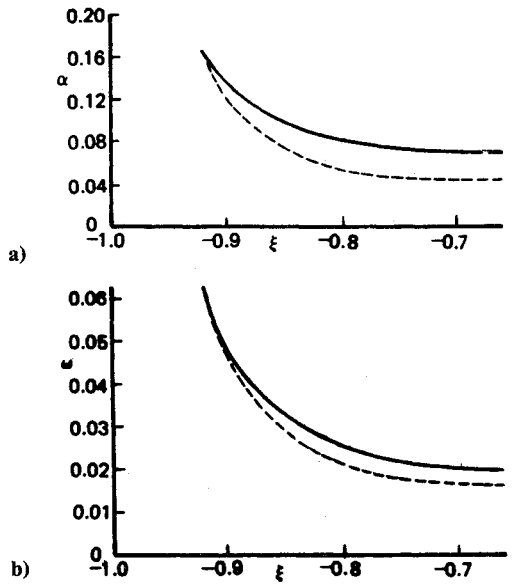

Fig. 4 Neutral stability curves (solid lines) and zarfs (dashed lines) for the leeward line of symmetry.

As can be seen, the computed amplification factors originate almost at the same x/c location and amplify differently depending on the choice of the frequency and may give different predictions of transition.

The accuracy of this procedure for computing transition was investigated for 13 cases of which 7 were for a sweep angle $\lambda = 49$ deg, 3 were for $\lambda = 55$ deg, and 3 were for $\lambda = 61$ deg. Some of the calculated and experimental results are presented in Figs. 3 and details of the calculations are summarized in Ref. 21.

V. Results and Discussion for the Prolate Spheroid

The stability calculations for the experimental data of Ref. 11 were performed with the procedure described in Sec. III.

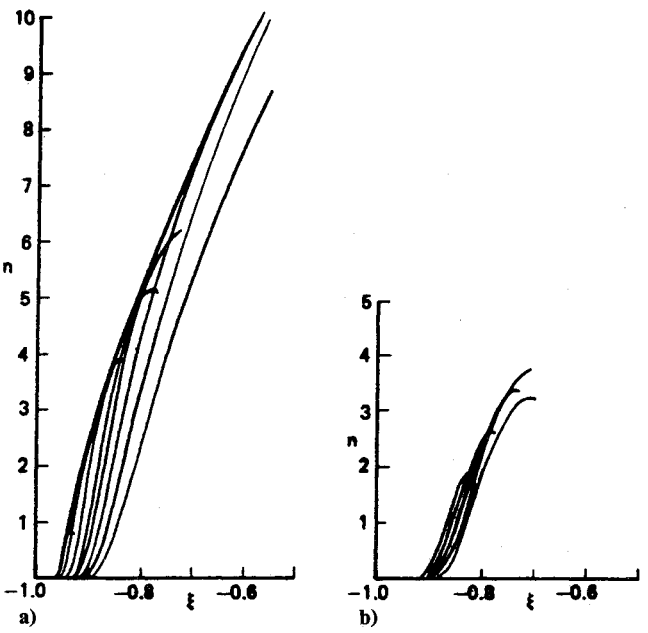

Fig. 5 Amplification factors on the leeward line of symmetry: a) two-dimensional disturbances ($\beta = 0$); b) three-dimensional disturbances ($\beta \neq 0$).

The calculation of transition on the windward and leeward lines of symmetry where $\theta = 0$ and 180 deg, respectively is somewhat similar to the calculation of transition in two-dimensional flows and is described in Sec. V A. The calculation of transition off the line of symmetry, however, requires that the calculation of the amplification rates Γ in which α_i and β_i are computed as a function of ξ, θ as the disturbance moves from (ξ_1, θ_1) which corresponds to the zarf to (ξ, θ); thus at each point of the path, α_i and β_i are computed as a function of ω. In addition, the value of Γ is computed for different disturbance angles in order to find the maximum amplification rate. As in the case of the swept wing, a search is also made for the critical frequency that leads to the most amplified integrated amplification rate, discussed in Sec. V B.

A. Results for the Line of Symmetry

On both lines of symmetry where the circumferential velocity component w is zero, stability calculations are somewhat similar to those in two-dimensional flows and can be performed by solving the eigenvalue problem for α, ω, and R or for α, β, ω, and R. The second choice leads to bifurcation on the leeward line of symmetry where the flow is decelerating but not on the windward line of symmetry where the flow is accelerating; bifurcation of such flows requires relatively high Reynolds numbers. The assumption made in both cases is that transition is caused by disturbances that originate on the line of symmetry. It is possible, however, that transition can also be caused by disturbances that originate off the line of symmetry. If they are amplified with negligible crossflow, their properties will be similar to those on the line of symmetry. In that event, it is necessary to determine which disturbance causes transition first. If the crossflow effect is not negligible, then the disturbances will have properties found in three-dimensional flows and, even if they manage to reach either line of symmetry, the transition will be triggered by those originating on the line of symmetry since the three-dimensional disturbances are more stable than two-dimensional ones.

Figures 4 and 5 present the results for the leeward line of symmetry; Fig. 6 presents those for the windward line. Figures 4 show the lower branch of the neutral stability curves (solid lines, $\beta = 0$) and zarfs (dashed lines, $\beta \neq 0$) with bifurcation taking place at $\xi = -0.9175$. According to Squire's theorem, the two-dimensional disturbances are more unstable than three-dimensional disturbances, so that the stability calcula-

tions for transition should be made without bifurcation. As a result, at a location $\xi = \xi_o$, the eigenvalues α, ω on the lower branch of the neutral stability curve were determined so that a dimensional frequency $\omega^*/2\pi$ can be specified at subsequent ξ locations and used in the calculation of the eigenvalues α_r, α_i as a function of Reynolds number or as ξ in order to determine the value of n from Eq. (6). This procedure led to one of the amplification curves of Fig. 5a and was repeated for other dimensional frequencies computed at different ξ locations in order to determine the first most amplified wave whose amplification reached the specified value of n. The results in Fig. 5a indicate that transition takes place at $\xi = -0.15$, which agrees well with the experimental value of -0.18.

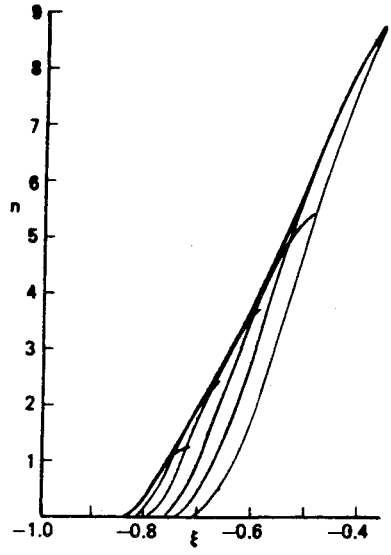

Fig. 6 Amplification factors for the windward line of symmetry ($\beta = 0$).

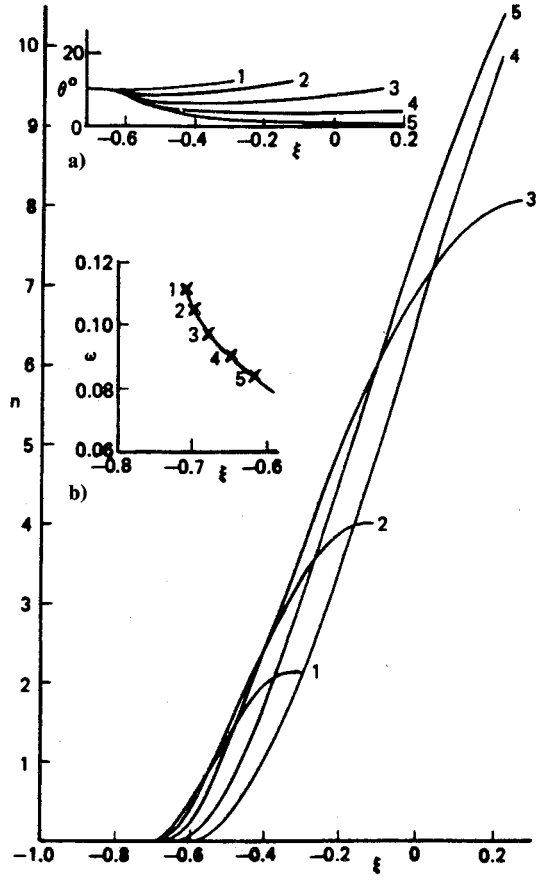

Fig. 7 Amplification factors computed with disturbances originating at $\theta = 10$ deg with five frequencies determined on the zarf (insert a) and with different wave propagation trajectories (insert b).

The results of Fig. 5b present amplification rates computed by the procedure just mentioned for three-dimensional disturbances. In this case, the calculations were initiated on the lower branch of the zarf by computing the eigenvalues α_r, β_r, and ω at $\xi = \xi_o$ so that the eigenvalues α and β can be computed for a specified dimensional frequency at subsequent ξ locations and transition can be computed from the integrated values of Γ. As can be seen from Fig. 5b, the results obtained with this procedure are considerably more stable than their counterparts in Fig. 5a and do not indicate transition.

Figure 6 shows the amplification rates on the windward line of symmetry obtained with the same procedure used to compute those shown in Fig. 5a. The envelope of the resulting curves indicates a value of $n = 10$ after $\xi = 0.30$, which does not agree well with the experimental data that indicate that transition occurs at $\xi = 0.13$. We note from the results in Figs. 5a and 6 that the amplification rates do form an envelope, as in two-dimensional flows, and suggest that the disturbances that cause the growth of instability and subsequently transition can be interpreted as Tollmien-Schlichting waves.

Figure 7 shows the amplification rates originated off the line of symmetry, at $\theta = 10$ deg, determined with the procedure to be discussed in Sec. V B. In this case, the disturbances with five frequencies resulting from the zarf and with their wave propagation trajectories varying as shown in the two inserts of Fig. 7 lead to 5 amplification rates. Of these, the frequencies denoted by 4 and 5 correspond to the critical values, and the wave with a frequency of 5 causes transition on the line of symmetry at $\xi = 0.20$, which is ahead of the wave that originated on the line of symmetry and caused transition to occur after $\xi = 0.30$. The disturbance with frequency 4 also causes transition. However, in this case, it takes place off the line of symmetry at $\xi = 0.18$. This indicates that in three-dimensional flows there can be more than one critical frequency emerging at a fixed θ location and leading to transition.

B. Results for Off the Line Symmetry

Off the line of symmetry, the flow is three-dimensional and, in general, the circumferential wave number β is not equal to zero. In addition, unlike the flow over an infinite swept wing, the flow cannot be assumed sectionally similar in either streamwise or circumferential direction. As a result, as the eigenvalues α and β are being computed to obtain the amplification rates for a specified dimensional frequency, wave angle, γ, and ξ location, the variation of the velocity profiles $\bar{u}$ and $\bar{w}$ in the circumferential direction must also be accounted for. To discuss this point further and describe our computational strategy off the line of symmetry, let us consider Fig. 8, in which C_o represents the fundamental stability curve of the flow in the sense that, to the left of it, all wall disturbances decay, whereas to the right, some, but not necessarily all, of

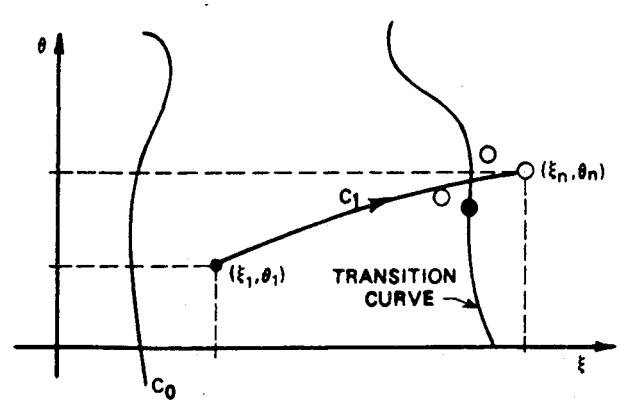

Fig. 8 Computational strategy.

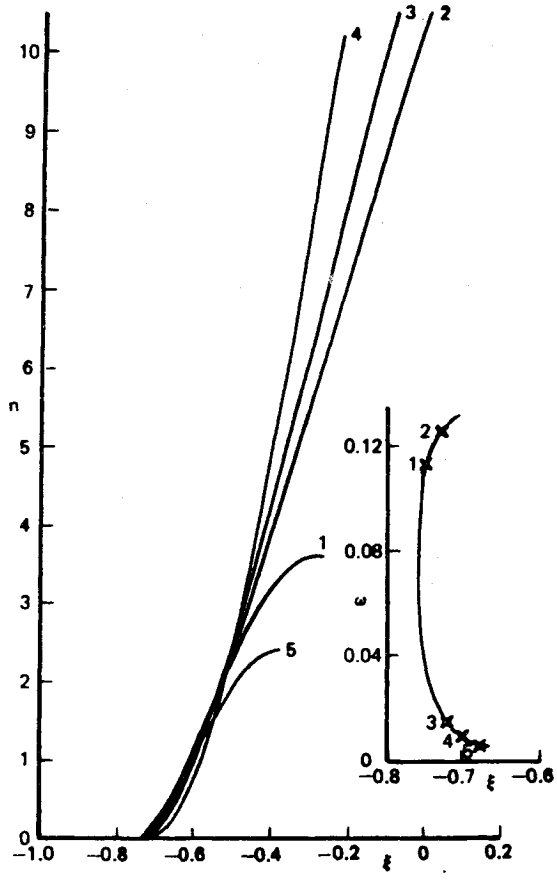

Fig. 9 Amplification factors with disturbances originating at $\theta = 20$ deg for five frequencies determined on the zarf (insert).

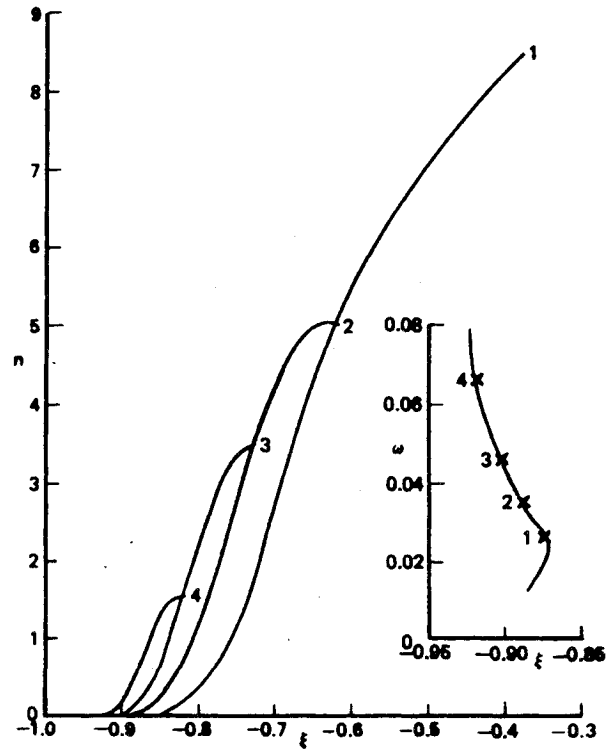

Fig. 10 Amplification factors with disturbances originating at $\theta = 150$ deg for four frequencies determined on the zarf (insert).

the disturbances grow as ξ increases. We assume that at point (ξ_1, θ_1), within a domain lying to the right of C_o, there passes a zarf and the appropriate value of ω on this zarf is ω_1 at this point. The curve C_1 passing through (ξ_1, θ_1) is the curve on which the growth factor is a maximum at the dimensional frequency $\omega_1^*/2\pi$ and this growth factor reaches a value of n at a point (ξ_n, θ_n). Similar curves originating at different ξ locations but the same θ location with dimensional frequencies $\omega_j^*/2\pi$ will lead to curves similar to C_1 with endpoints denoted by circles except that the location and the value of n at the end of the integration process will be different. According to the philosophy of the e^n method, the first such wave to increase in amplitude by a factor of e^n as ξ increases is said to be a critical transition wave and the corresponding value of $\xi_T(\theta)$ is claimed to be a good approximation to the onset portion of transition. Thus, by varying θ, and computing amplification rates corresponding to zarf frequencies at different ξ locations, an estimate of the transition curve on the body of revolution under consideration is obtained.

Figure 9 shows the integrated amplification rates with disturbances originating at $\theta = 20$ deg for five frequencies determined on the zarf. We note that those denoted by 1 on the upper branch and 5 on the lower branch of the zarf do not lead to amplified waves, but those designated by 2 on the upper branch and 3 and 4 on the lower branch do. Of these three frequencies, the one designated by 4 corresponds to the critical frequency that causes transition.

Figure 10 shows the results for $\theta = 150$ deg. Reference 21 presents similar results for $\theta = 40$, 80, and 120 deg. In this case, the shape of the zarf is different from all of the other zarfs. Except for the frequency designated by 1, none of the other frequencies lead to high-amplification rates. It appears that, as the value of θ increases from its value on the windward line of symmetry, the critical frequencies that were on the lower branch of the zarf shift to the upper branch; with further increase in θ, as the leeward line is approached, this trend reverses and the critical frequencies begin to migrate toward the inflection point of the zarf.

Figures 11 show the trajectories of the wave propagation computed with different frequencies originated at specified values of θ corresponding to 10, 20, 40, 80 (Fig. 11a), 120, and 150 deg (Fig. 11b). We note from those for $\theta = 10$ deg that the trajectories of the waves with frequencies 1 and 2 have small angles, suggesting that their behavior is similar to those already discussed in Sec. V A; the behavior of the disturbances, especially those corresponding to frequencies 4 and 5, are more two dimensional than three dimensional. For $\theta = 20$ deg, the trajectories with frequencies 3, 4, and 5 have angles comparable to others originated at values of $\theta > 20$ deg. It is interesting to note that the results for $\theta = 40$ deg, the disturbance angle corresponding to the most amplified wave is not the biggest one since in this case the disturbance with frequency of 1 leads to transition.

As the leeward line of symmetry is approached, however, a behavior similar to that found near the windward line of symmetry for some frequencies is observed. For example, for the disturbances that originate at $\theta = 150$ deg, those with frequencies of 1, 2, and 3 have initially very small angles that remain relatively constant over a distance on the body before they increase. This behavior again suggests that the disturbances with these frequencies are nearly two dimensional but become three dimensional later, unlike the behavior of nearly two-dimensional disturbances near the windward line of symmetry. The reason for this behavior is due to the difference in the crossflow velocity profiles. It is also interesting to note that the disturbance that originated at $\theta = 150$ deg with a frequency of 4 is three dimensional and, as expected, is more stable than those with frequencies of 1, 2, and 3.

Figure 12 presents a summary of the stability/transition and boundary-layer calculations. The first curve on the left side corresponds to the location of the critical frequencies on the zarf. We note from this curve that its behavior, as we approach the leeward line of symmetry, begins to exhibit a difference at $\theta \geq 160$ deg from those at $\theta < 160$ deg. This difference is due to the effect of the crossflow velocity profiles that,

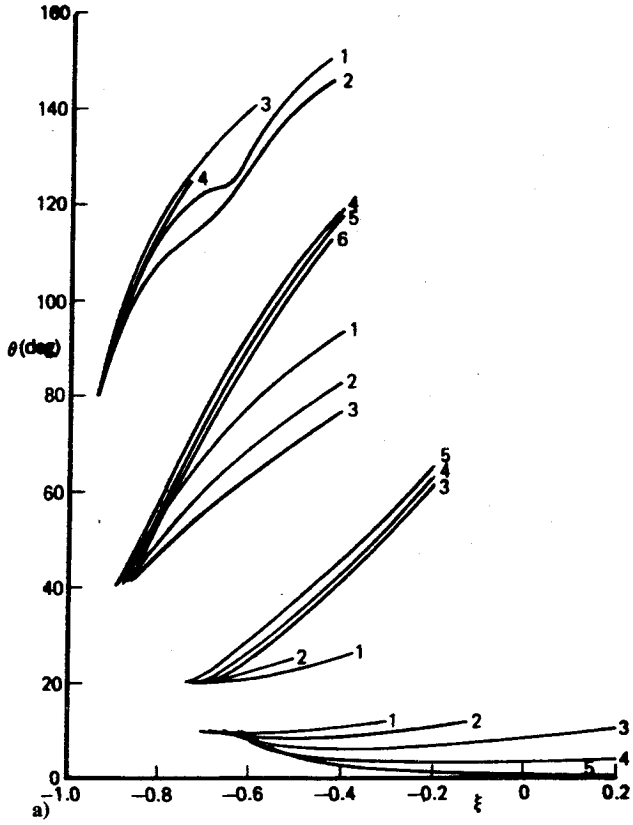

Fig. 11 Trajectories of the wave originating at specified values of θ with different frequencies: a) θ from 10 to 80 deg; b) θ for 120 and 150 deg.

as those for $\theta = 150$ deg, begin to exhibit significant changes with ξ as the calculations progress downstream of the zarf. To the right of this curve is the dashed line that corresponds to the locus of transition location computed with the present method for $n = 10$. The experimental values are denoted by the solid line to the right of this computed transition curve.

Figure 12 also presents the separation line for this angle of attack, which, as in the $\alpha = 6$ deg case studied by Cebeci and Su[9] is open and corresponds to a skin-friction line, as discussed in detail in Ref. 9. The lines referred to as the terminal lines are defined by the breakdown of the boundary-layer calculations, which, in this case, correspond to the vanishing of the streamwise wall shear. This is due to the formulation of the boundary-layer problem in direct form and can be avoided

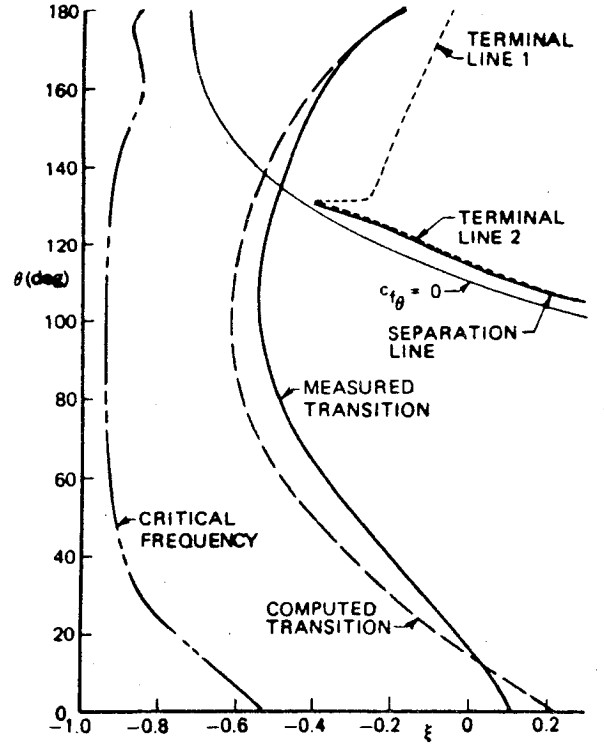

Fig. 12 Calculated and experimental transition locations on the prolate spheroid at $\alpha = 10$ deg.

by the use of inverse procedures in which the external velocities are computed as part of the solution.

Conclusions

A method, based on a combination of interactive boundary-layer and linear-stability theories has been developed and evaluated for the calculation of the three-dimensional flows on infinite swept wings and prolate spheroids. For infinite swept wings, emphasis has been placed on the calculation of the onset of transition as influenced by Reynolds number and sweep angle. The stability approach is based on spatial amplification theory with the eigenvalue procedure formulated so that the relationship between the two wave numbers is determined as part of the computational method. The usefulness of the neutral stability curves (zarfs) for the critical frequency and its location needed in the e^n method has been clearly demonstrated for three-dimensional flows. In particular, the critical frequency occurs very close to the leading edge of the wing, at least in the present cases, and the zarfs facilitate their correct calculation and avoid uncertainties associated with the choice of magnitude and location of the critical frequency. The predicted locations of transition are shown to be in close agreement with measurements for all of the sweep angles, angles of attack, and speeds considered in the experimental data. It should be noted that the present method predicts transition in regions where crossflow dominates the flowfield as well as in regions where it is weak and where the flowfield is dominated by the Tollmien-Schlichting waves.

The agreement between calculated and measured results is also impressive for the prolate spheroid at $\alpha = 10$ deg. The value of n was taken as 10 to compensate for the solution of the boundary-layer equations with a prescribed pressure distribution based on the inviscid flow calculation. It is interesting to note that the transition on the line of symmetry can be caused by disturbances that originate off the line of symmetry. It is also noted that there can be more than one critical frequency in three-dimensional flows that can lead to transition. The direction of wave propagation used in the eigenvalue formulation is very sensitive to flow reversals in crossflow velocity profiles and plays an even more important role in the

calculation of transition on a body of revolution than on a swept wing.

Acknowledgments

This work was made possible by financial support provided by the Office of Naval Research over many years. We are glad to acknowledge the encouragement provided by R. Whitehead and hope that the results of this paper justify it. More recently, support from David Taylor Research Center under the present contract allowed this work to continue and the method to be extended and evaluated for the configurations described. Some of the concepts upon which the methodology are based stem from discussions with K. Stewartson, whose untimely death prevented him from participating in the application of his ideas.

References

[1]Smith, A. M. O., and Gamberoni, N., "Transition, Pressure Gradient, and Stability Theory," *Proceedings of the International Congress of Applied Mechanics*, Brussels, Vol. 4, 1956, p. 234.

[2]Van Ingen, J. L., "A Suggested Semi-Empirical Method for the Calculation of the Boundary-Layer Region,"VTH71, VTH74, Delft, Holland, 1956.

[3]Bushnell, D. M., Malik, M. R., and Harvey, W. D., "Transition Prediction in External Flows via Linear Stability Theory," IUTAM Symposium Transsonicum III, Göttingen, Germany, 1988.

[4]Wazzan, A. R., "Spatial Stability of Tollmien-Schlichting Waves," *Progress in Aerospace Sciences*, Vol. 16, Pergamon, New York, 1975, pp. 99-127.

[5]Cebeci, T., and Egan, D. A., "Prediction of Transition Due to Isolated Roughness," *AIAA Journal*, Vol. 27, 1989, pp. 870-875.

[6]Cebeci, T., "Essential Ingredients of a Method for Low Reynolds-Number Airfoils, *AIAA Journal*, Vol. 27, 1989, pp. 1680-1688.

[7]Malik, M. R., Wilkinson, S. P., and Orzag, S. A., "Instability and Transition in Rotating Disk Flow" *AIAA Journal*, Vol. 29, 1981, pp. 1131-1138.

[8]Malik, M. R., and Poll, D. I. A., "Effect of Curvature on Three-Dimensional Boundary-Layer Stability," *AIAA Journal*, Vol. 23, 1985, pp. 1362-1369.

[9]Cebeci, T., and Su, W., "Separation of Three-Dimensional Laminar Boundary Layers on a Prolate Spheroid" *Journal of Fluid Mechanics*, Vol. 191, 1988, pp. 47-77.

[10]Arnal, D., and Juillian, J. C., "Three-Dimensional Transition Studies at ONERA/CERT," AIAA Paper 87-1335, June 1987.

[11]Meier, H. U., and Kreplin, H. P., "Experimental Investigation of the Boundary-Layer Transition on a Body of Revolution," *Zeitschrift für Flugwiss Weltraumforsch*, Vol. 4, 1981, p. 65.

[12]Cebeci, T., Clark, R. W., Chang, K. C., Halsey, N. D., and Lee, K., "Airfoils with Separation and Resulting Wakes," *Journal of Fluid Mechanics*, Vol. 163, 1986, pp. 323-347.

[13]Cebeci, T., Kaups, K., and Khattab, A. A., "Separation and Reattachment Near the Leading Edge of a Thin Wing," *IUTAM Symposium, Boundary-Layer Separation*, edited by F. T. Smith and S. N. Brown, Springer-Verlag, Heidelberg, Germany, 1987.

[14]Cebeci, T., and Bradshaw, P., *Momentum Transfer in Boundary Layers*, McGraw-Hill/Hemisphere, Washington, DC, 1977.

[15]Malik, M. R., "COSAL—A Black Box Compressible Stability Analysis Code for Transition Prediction in Three-Dimensional Boundary Layers," NASA CR-165 925, 1982.

[16]Mack, L. M., "Stability of Three-Dimensional Boundary Layers on Swept Wings at Transonic Speeds," IUTAM Symposium, Transsonicum III, Göttingen, Germany, 1988.

[17]Cebeci, T., and Stewartson, K., "Stability and Transition in Three-Dimensional Flows," *AIAA Journal*, Vol. 18, 1980, pp. 398-405.

[18]Nayfeh, A. H., "Stability of Three-Dimensional Boundary Layers," *AIAA Journal*, Vol. 18, 1980, pp. 406-416.

[19]Cebeci, T., and Stewartson, K., "On the Prediction of Transition in Three-Dimensional Flows," *Proceedings of IUTAM Symposium on Laminar-Turbulent Transition*, edited by R. Eppler and H. Fasel, Springer-Verlag, New York, 1980, pp. 243-252.

[20]Cebeci, T., Khattab, A. A., and Stewartson, K., "On Nose Separation," *Journal of Fluid Mechanics*, Vol. 97, 1980, pp. 435-454.

[21]Cebeci, T., and Chen, H. H., "Prediction of Transition on Airfoils with Separation Bubbles, Swept Wings, and Bodies of Revolution at Incidence," *Numerical and Physical Aspects of Aerodynamic Flows IV*, edited by T. Cebeci, Springer-Verlag, New York, 1990, pp. 303-320.

[22]Pfenninger, W., "Laminar Flow Control," Paper 3, *Special Course on Concepts for Drag Reduction*, AGARD Rep. 654, 1977.

[23]Gaster, M., "On The Flow Along Swept Leading Edges," *Aeronautical Quarterly*, Vol. 18, pp. 165-184.

[24]Poll, D. I. A., "Transition in the Infinite Swept Attachment-Line Boundary Layer," *Aeronautical Quarterly*, Vol. 30, 1979, pp. 607-628.

[25]Hall, P., Malik, M. R., and Poll, D. I. A., "On the Stability of Infinite Swept Attachment Line Boundary Layer," *Proceedings of the Royal Society of London*, Vol. A 935, 1984, pp. 229-245.

[26]Cebeci, T., and Chen, H. H., "A Numerical Method for Predicting Transition in Three-Dimensional Flows by Spatial Amplification Theory," AIAA Paper 91-1606, 1991.